

ULTRA-HIGH-RESOLUTION OBSERVATIONS OF INTERSTELLAR Na I AND Ca II K TOWARD THE HIGH GALACTIC LATITUDE STAR HD 28497

J. CHRIS BLADES, M. S. SAHU, AND LIDA HE¹

Space Telescope Science Institute, 3700 San Martin Drive, Baltimore, MD 21218

AND

I. A. CRAWFORD, M. J. BARLOW, AND F. DIEGO

Department of Physics and Astronomy, University College London, Gower Street, London, WC1E 6BT, England, UK

Received 1996 July 1; accepted 1996 October 8

ABSTRACT

We present very high resolution (0.32 km s^{-1}) spectra of interstellar Na I D1, D2, and Ca II K absorption toward HD 28497 obtained with the Ultra-High-Resolution Facility at the 3.9 m Anglo-Australian Telescope. The star is located in projection in a highly disturbed interstellar region close to a number of identified features including the high galactic latitude molecular cloud MBM 20, the large Orion-Eridanus shell, seen in H α and H I 21 cm maps, and a filamentary loop structure between $v_{\text{LSR}} = -12$ and -4 km s^{-1} in the Berkeley H I 21 cm survey and visible on the *IRAS* 100 μm map.

Toward HD 28497 we detect 13 absorption components in the Na I spectra, to a column density limit of $2 \times 10^{10} \text{ cm}^{-2}$, and 10 in Ca II K over a velocity range of $\sim 70 \text{ km s}^{-1}$. Four absorption components in the Na I spectra show *s*-resolved hyperfine structure with *b*-values from 0.31 to 0.40 km s^{-1} and column densities from 4.0 to $14 \times 10^{10} \text{ cm}^{-2}$. If we assume the clouds represented by these components have no internal turbulent velocities, their temperatures would range between 134 and 227 K. One of these hyperfine split (hfs) components, at $v_{\text{LSR}} = -11.1 \text{ km s}^{-1}$, shows significant temporal variation in equivalent width compared to earlier (1977) observations, making this the first interstellar sight line outside the Vela supernova remnant to show a time-varying component. The feature may be associated with the filamentary loop structure seen in this region.

There is poor correspondence between the Na I and Ca II profiles: we do not detect narrow Ca II profiles to the four hfs Na I components, and only three of the well-resolved components have the same Ca II and Na I radial velocities and consistent *b*-values. One of these components, at $v_{\text{LSR}} = -30.0 \text{ km s}^{-1}$, has a low Na I/Ca II ratio and arises in a region where turbulent motions dominate—properties consistent with the hypothesis that the cloud lies close to HD 28497. In general, however, the Na I and Ca II occupy different gaseous phases in the ISM.

We have compared our data with 21 cm emission profiles obtained from the recent Leiden/Dwingeloo H I survey. Based on agreement in the velocities, the Na I/Ca II ratio, and the kinetic temperatures, we conclude that the component at $v_{\text{LSR}} = -7.5 \text{ km s}^{-1}$ is associated with the front side of the large, expanding Orion-Eridanus shell. Unexpectedly, the molecular cloud MBM 20 is not detected either in our absorption spectra or in the H I profiles, indicating that HD 28497 lies away from the core of MBM 20.

Apart from the two features at -11 and -7.5 km s^{-1} there is almost no agreement between the H I profiles and the optical spectra. Although we cannot rule out the possibility that most of the H I lies behind the star, this explanation seems unlikely because many of the H I features have previously been attributed to foreground phenomena. The beam sizes of the H I and the optical studies are quite different and this suggests a different explanation, namely that the physical sizes of the interstellar structures we detect in Na I and Ca II are not extensive enough to be detected in H I. If so, this raises questions about the usefulness in general of combining results obtained from H I 21 cm studies with results obtained from optical (or ultraviolet) studies of the interstellar gas.

Subject headings: atomic data — ISM: abundances — ISM: kinematics and dynamics — stars: individual (HD 28497)

1. INTRODUCTION

In this paper, we present results from a new spectroscopic study of interstellar gas toward HD 28497. This star at $l = 208^\circ 8$ and $b = -37^\circ 4$ is located in projection close to the edge of a dense *IRAS* 100 μm emission core associated with the high galactic latitude cloud MBM 20 (Magnani, Blitz, & Mundy 1985; Penprase 1993), and one purpose in studying this sight line was to probe the diffuse molecular cloud specifically associated with the IR cirrus. The star is

known to exhibit a complex interstellar spectrum, and previous optical studies have included Na I, at a velocity resolution of 0.9 km s^{-1} , and Ca II, at a velocity resolution of $\sim 15 \text{ km s}^{-1}$ (Shull, York, & Hobbs 1977; hereafter SYH). Penprase (1993) also studied these lines, at a velocity resolution of 3.5 km s^{-1} . The Na I absorption line spectrum was shown to consist of four major velocity components with substantial column density variations that appear to be correlated with cloud velocity, according to Shull & York (1977), who reported on ultraviolet observations of the star made with the *Copernicus* satellite. Molecular hydrogen is also detected at two different velocities toward

¹ On leave from Physics Department, Rensselaer Polytechnic Institute, Troy, NY 12180.

HD 28497. As we shall show, at our resolution the sight line is considerably more complicated than revealed previously. Despite the additional complexity, the clouds have small equivalent widths and are well resolved to allow very precise measurements of the column densities and b -values.

HD 28497 (=SAO 149674 = DU Eri = HR 1423 = 28 Eri) is classified as a normal emission-line Be star with spectral type B2V:ne, $V = 5.6$, and $v \sin i = 230 \text{ km s}^{-1}$ (Slettebak 1982). The *IRAS* infrared excess for HD 28497 at 12 and 25 μm was shown by Whitelock, Feast, & Catchpole (1989) to lie in the range expected for normal Be star free-free excesses. The star is known to vary both optically and in the near-IR (Ashok et al. 1984; Whitelock et al. 1989), a signature of Be stars. The distance to HD 28497 is not well determined; Lesh (1968) reports that the star has spectral peculiarities but nevertheless assigns an approximate M_v of 5.60 from the calibration for normal stars and obtains a distance of 465 pc, while Penprase (1993) assigned a distance of 740 pc with an uncertainty of a factor 2. The radial velocity (heliocentric) for the star has been determined to be $+12 \text{ km s}^{-1}$ by Abt & Biggs (1972) which corresponds to a v_{LSR} of -5.7 km s^{-1} .

As we mentioned earlier, we expected to use the star to probe gas associated with MBM 20. The region around this high-latitude cloud has been extensively mapped in CO(1 \rightarrow 0) (Magnani et al. 1985), in OH and CH by Sandell et al. (1981), in H₂CO by Goss et al. (1980), in CO(2 \rightarrow 1) by de Vries et al. (1984), and in C¹⁸O by Liljestrom (1991). In all these molecular transitions, the MBM 20 cloud is found to have a v_{LSR} ranging between $+0.02$ to $+0.8 \text{ km s}^{-1}$. MBM 20 has a central condensation in CO, and a nebulous object found close to the CO(1 \rightarrow 0) peak has previously been suggested to be a T Tauri or Herbig Ae/Be star, from its association with the nebulosity (Sandell et al. 1981). Although at high galactic latitude, the distance to MBM 20 is estimated to be only 100–130 pc (Penprase 1992), so that its height above the galactic plane is less than 80 pc. The spectroscopic class and distance of the object discovered by Sandell et al. remain to be established. However, HD 28497 clearly lies beyond MBM 20.

HD 28497 also lies in projection within the Orion-Eridanus bubble, a large expanding shell (radius = 140 pc, expansion velocity = 15–23 km s^{-1}) of ionized (H α) emitting and neutral (H I) gas, located between $160^\circ < l < 240^\circ$ and $-60^\circ < b < 0^\circ$ (Reynolds & Ogden 1979). Further, the star lies close to a 21 cm loop structure visible at $v_{\text{LSR}} \sim -11 \text{ km s}^{-1}$ on the Berkeley H I survey maps (Heiles & Habing 1974). This H I feature has been studied by Taylor, Taylor, & Vaile (1982) and by Liljestrom & Mattila (1988) and has been tentatively interpreted as gas associated with MBM 20. The Eridanus X-ray enhancement, a large and striking feature in the soft X-ray sky, consists of two components (Burrows et al. 1993) and one of the components (EXE-2, at $l = 210^\circ$ and $b = -43^\circ$) and seen only in the $\frac{1}{4}$ keV data lies close to the sight line of HD 28497. The presence of H α filaments, the H I loop, the expanding H I shell, the enhanced soft X-ray emission, and the star-forming MBM molecular cloud in the region, all point to a complex line of sight (see Fig. 9b, Burrows et al. 1993, and Brown, Hartmann, & Burton 1995).

2. OBSERVATIONS AND DATA REDUCTION

HD 28497 was observed on 1994 January 23 and 24 using the UHRF (Diego et al. 1995) at the coudé focus of the 3.9

m Anglo-Australian Telescope. The configuration of the spectrograph was set to give close to the highest achievable resolution, namely, $R = 938,000 \pm 15,000$ or 0.32 km s^{-1} . We used the 35 slice image slicer (Diego 1993) at the entrance aperture in an observing strategy similar to that described by Barlow et al. (1995) for their Ca II observations for ζ Oph. We masked the image slicer down to give 18 slices on the detector which allowed for the simultaneous detection of the interorder background on either side of the stellar spectrum.

The detector was a blue-coated Thompson CCD (1024 by 1024 pixel format) with a pixel size of 19×19 microns, corresponding to 0.0025 \AA or 0.13 km s^{-1} in the dispersion direction. The width of each individual slice produced by the image slicer is about 30 pixels, and the 18 slices filled over half the detector format. The order background filled the remainder. The entire CCD was read out with 8 times binning in the direction perpendicular to the dispersion.

The instrumental set-up gave a wavelength coverage of 2.5 \AA , requiring separate exposures for each of the Na I D lines and for Ca II K. Individual exposures were normally of 1200 s duration, and the total integration times were 60 minutes for D1, 40 minutes for D2, and 78.3 minutes for Ca II K. We used two different grating settings for the Ca II K lines so only the central part of this spectrum (in the range between -80 and 0 km s^{-1} LSR) has the full integration. The seeing was measured to be 1.2 arcsec on both nights. Comparison exposures using a Th-Ar lamp were used to establish the wavelength scale and showed that the plate scale is linear with wavelength over the 2.5 \AA coverage (Barlow et al. 1995). Measurements of the 6328.160 \AA stabilized He-Ne laser line taken during the observing run confirmed that we achieved a resolution of 0.32 km s^{-1} (FWHM).

Individual integrations were combined after cosmic-ray events and the interorder background had been removed. A scattered light correction of 3.5% was applied to the data, derived from observations of a highly saturated D line in a different star (HD 24263) recorded during the same period. The spectra were normalized by fits of straight lines to sections without telluric or interstellar absorption. Telluric absorptions around the D line region were removed by dividing by a UHRF telluric template spectrum of α Eri, which was rescaled so that the optical depth of its individual telluric features matched those of unblended telluric lines in the spectra. Rest wavelengths in air of 5895.9234 \AA for D1, 5889.9512 \AA for D2, and 3933.663 \AA for Ca II K were adopted from Morton (1991). The normalized spectra are shown in Figure 1. The signal-to-noise ratios derived from the rms fluctuation in the continuum are 60 for D1, 30 for D2, and for Ca II K, 30 for $v_{\text{LSR}} < 0 \text{ km s}^{-1}$ and 20 for $v_{\text{LSR}} > 0 \text{ km s}^{-1}$.

We used the method of profile fitting developed by Welty, Hobbs, & Kulkarni (1994) to derive the properties of the individual interstellar clouds. The essential assumptions are that each cloud is homogeneous and can be described by a column density N , radial velocity v , and a Gaussian line of sight velocity dispersion characterized by the line width parameter $b = (2KT_t/m + 2v_t^2)^{1/2}$, where v_t is the rms (Gaussian) turbulent velocity along the line of sight. The intrinsic line profiles were calculated assuming a minimum number of velocity components and were then convolved with the instrumental response. The three parameters (N , v , b) for each cloud were then determined by an iterative, non-

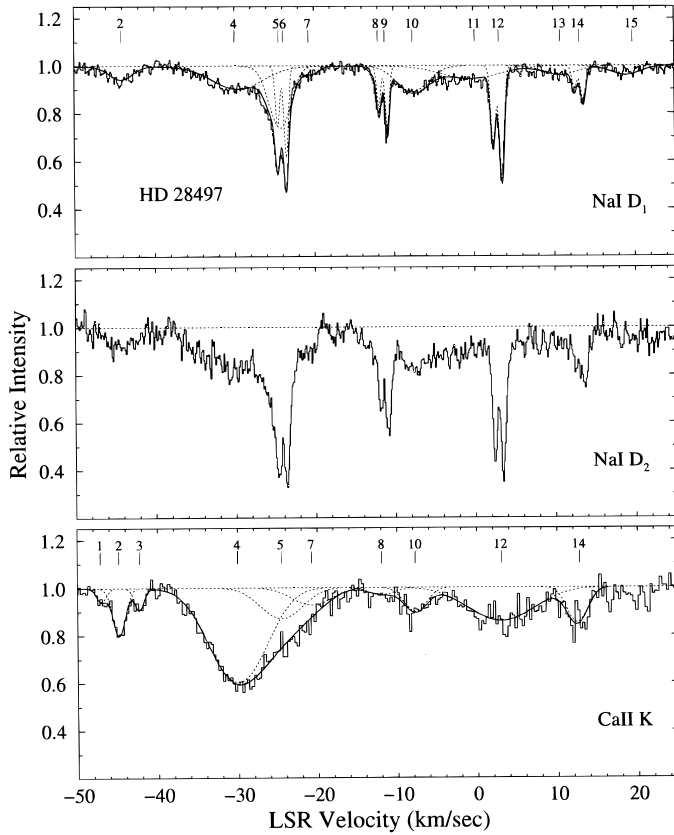


FIG. 1.—Normalized spectra of Na I and Ca II toward HD 28497 obtained at 0.32 km s^{-1} resolution. Note the four prominent narrow Na I clouds showing hyperfine splitting and numerous broad clouds in this species and in Ca II. The difference between the Na I and Ca II K profiles are striking. A 13 component model has been fitted to Na I data and the individual components (*dashed lines*) as well as the integrated fit (*solid lines*) are shown. A 10 component model has been fitted to the Ca II K line.

linear, least-square fit to the observed profile. The model fitting revealed 13 different velocity components for Na I D lines. In fitting the Ca II K line we started with the 13 component D line model and then made modifications through trial and error. The narrow Na I components do

not have Ca II counterparts so these were removed from the model. However, at least some of the broader Ca II features appear to be common with Na I, although their b -values are often quite different, and so their radial velocities were adopted from the D-line model. We identify 13 discrete velocity features in Na I and 10 features in Ca II K. The parameters are listed in Table 1. The Na I (N , b) values are an average of the values of Na I D1 and D2 lines. The errors for the Na I were calculated based on the fluctuations from this average value. For the case of the Ca II profiles, errors, were computed by determining an extreme range of (N , b) values which gave fits that were within the N/S values at every point on the observed profiles. The fitted profiles are shown as solid lines in Figure 1, while the dashed lines represent the contribution from each individual component. The total column density derived from model fitting is $10.4 \times 10^{11} \text{ cm}^{-2}$ for Na I and $13.2 \times 10^{11} \text{ atoms cm}^{-2}$ for Ca II.

We have compared our Na I D2 and Ca II K profiles with those obtained by SYH for D2 and by Hobbs (1984) for Ca II K in Figure 2. SYH quoted their resolution to be 0.9 km s^{-1} ; however, their achieved resolution must have been lower, otherwise hyperfine splitting should have been resolved in their study. The Ca II K line profiles show good agreement, even though Hobbs's (1984) resolution is 5.5 km s^{-1} and our data are at a lower signal-to-noise ratio; our total equivalent width is $114 \pm 7 \text{ mÅ}$ compared with 135 mÅ from Hobbs (1984). For Na I D2, bearing in mind that the PEPSIOS data do not resolve hyperfine splitting, and that SYH did not remove telluric absorption, the profile agreement is again reasonable. The difference near $v_{\text{LSR}} = -31.5 \text{ km s}^{-1}$ could be due to the presence of a strong telluric feature while the significant change for the -11.1 km s^{-1} feature (component 9) is probably due to temporal variation in this cloud (see § 3.1.1). The total equivalent width for all the D2 components from our study is 167 mÅ compared to 187 mÅ from SYH, and these are consistent measures bearing in mind that SYH did not remove telluric absorption. For the narrow Na I velocity components, our internal velocity uncertainty is 0.1 km s^{-1} , based on the comparison between D2 and D1. A comparison with the

TABLE 1
MODEL FIT PARAMETERS TO THE Na I D AND Ca II K LINES

COMPONENT	V_{lsr} (km s^{-1})	Na I $N(10^{11})^a$ (cm^{-2})	b^a (km s^{-1})	V_{lsr} (km s^{-1})	Ca II $N(10^{11})^a$ (cm^{-2})	b^a (km s^{-1})
1.....	-47.0	0.13a	1.0b
2.....	-44.1	0.40a	1.8a	-44.8	0.64a	1.1b
3.....	-42.3	0.21a	0.8a
4.....	-29.9	1.61a	4.6a	-30.0	6.31a	4.6b
*5.....	-24.5	1.7:	1.5:	-24.5	1.4:	3.5:
6.....	-23.9	0.98a	0.32a			
*7.....	-20.9	0.24c	1.4c	-20.7	0.7:	3.5:
*8.....	-12.1	0.2:	1:	-11.9	0.2:	2.5:
9.....	-11.1	0.63a	0.31a			
10.....	-7.5	1.06a	2.8a	-7.7	0.57a	2.1b
11.....	-0.2	0.99a	5.0a			
12.....	+3.1	1.44a	0.37a	+3.0	2.33a	5.7a
*13.....	+10.7	0.4:	3:			
14.....	+13.2	0.41a	0.40a	+12.5	0.76a	1.8b
*15.....	+20.0	0.35:	2.5:			

NOTE.—* Component not well resolved in the spectra.

^a (a) error < 10%; (b) error 10 to 30%; (c) error > 30%. See § 2. : uncertain, component very weak or badly blended.

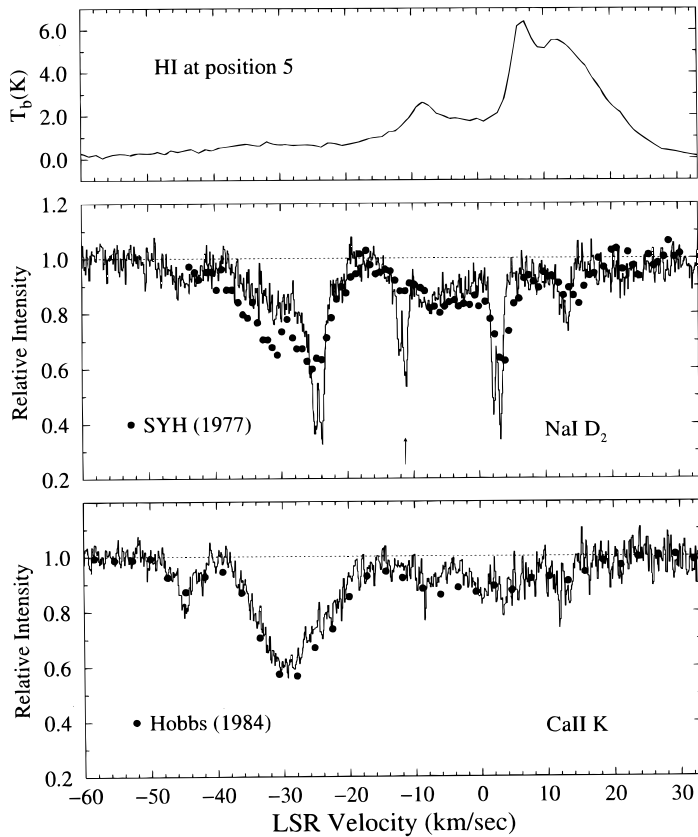


FIG. 2.—The top panel shows the H I profile at position 5 (see Table 3). Compare this to the Na I D2 and the Ca II K absorption profile shown in the middle and lower panels, respectively. Note that except for the broad -7.5 km s^{-1} component, the H I profile shows no common component with the Na D2 spectra. The middle panel shows a comparison of our Na I D2 AAT UHRF profile (solid line) with Na I D2 spectrum (dots) of Shull, York, & Hobbs (1977; SYH). The D2 profiles differ in two ways: (1) the prominent feature at -11.1 km s^{-1} is absent in SYH (shown by an arrow) and we suggest in § 3.1.1 that this is due to a temporal variation of the total equivalent width of the cloud and indicates the presence of a small-scale structure. The mismatch in profiles near -31 km s^{-1} may be due to a prominent telluric absorption that we have removed from our data but was not removed by SYH. The lower panel shows the excellent agreement between our Ca II K spectrum and that of Hobbs (1984) (dots).

PEPSIOS profile shows the following agreement: for the -24.5 km s^{-1} feature SYH obtained -24.7 km s^{-1} ; for the $+3.1 \text{ km s}^{-1}$ feature SYH obtained $+3.9 \text{ km s}^{-1}$; and for the $+13.2 \text{ km s}^{-1}$ feature SYH obtained $+15.1 \text{ km s}^{-1}$ suggesting a small plate-scale change. Our D1 and D2 velocities are very consistent internally, indicating the error may arise in the lower resolution SYH data.

3. RESULTS AND DISCUSSIONS

The morphology of the Na I absorption profile and the striking differences between this profile and that of Ca II are the immediate and remarkable features of the spectra toward HD 28497 and merit a few general remarks. Clearly, the very high resolution of the UHRF is revealing directly the actual widths of the absorption lines and, thereby, is providing a capability to characterize different physical domains of the ISM. With the UHRF we are now detecting different components of the diffuse ISM, such as cold neutral clouds, or warm intercloud gas. We can determine physical parameters such as temperatures and turbulence, and investigate the coexistence of different species within the different components. Also, we have the potential to

make very precise measurements of depletion levels and abundances—provided overlapping velocity components and saturation effects do not interfere.

The data lend themselves to interpretation in the context of the McKee & Ostriker (1977) three-phase model of the ISM in which the neutral ISM is contained in clouds with cold dense cores (the cold neutral medium, CNM) with densities $n \sim 10\text{--}1000 \text{ cm}^{-3}$ and $T \sim 80 \text{ K}$ and which are enveloped by a tenuous warm medium ($T \sim 8000 \text{ K}$) with both neutral (WNM) and ionized (WIM) parts. The hot ionized environment at $T \sim 5 \times 10^5 \text{ K}$ forms the background medium in which the other two phases are embedded. Most of the mass of the ISM is in clouds, both cold and warm, which have small volume-filling factors.

3.1. The Optical Spectra

Toward HD 28497, we find that the Na I components fall into two groups. There are four narrow components (CNM clouds) which show s -resolved (McNutt & Mack 1963) hyperfine structure, superposed on an undulating background of broad and poorly resolved absorption features (WNM or WIM clouds). Overall, we have identified 13 Na I velocity components over an LSR velocity range from -50 to $+20 \text{ km s}^{-1}$, and their positions are shown as tick marks above the Na I D1 profile in Figure 1.

For the case of the four hfs lines (components 6, 9, 12, and 14), the best-fitting b -values range from 0.31 to 0.40 km s^{-1} . In the absence of turbulence, these b -values correspond to kinetic temperatures between 134 and 227 K . These temperatures are upper limits since any turbulent motions would also contribute to the measured b -values. In § 3.1.2 we argue that turbulent velocity contributions may indeed be present, based on a comparison with kinetic temperature values established from H_2 measurements. The column densities of these four components range from 4 to $14 \times 10^{10} \text{ cm}^{-2}$. For the broader features, the best-fitting b -values range from 0.8 to 5 km s^{-1} , although typical values are in the range from 1.5 to 3 km s^{-1} , and the column densities are in the range from 2 to $50 \times 10^{10} \text{ cm}^{-2}$. We point out that the model fit to these broad and poorly defined interstellar components is a plausible fit but by no means the only one possible. Probably there are additional and weaker features that we are missing but which higher S/N would reveal.

As we have mentioned already, at a first glance of Figure 1, there is not a good match between the Na I and the Ca II absorption profiles—suggesting a poor correspondence between the two species. Narrow Ca II counterparts [i.e., $b(\text{Ca II}) \lesssim b(\text{Na I})$] to the four hfs clouds are not detected, which is consistent with the view that these are cold neutral clouds. On the other hand, a close comparison of the Ca II and Na I profiles shows six components with the same velocities within the resolution of the spectra: these are components 4, 5, 7, 8, 10, and 12. Three of these components, 5, 7, and 8, are blended features in both Ca II and Na I. They have $b(\text{Ca II}) > b(\text{Na I})$ which suggests the species do not coexist directly in the same clouds. If the species are associated in the same interstellar region, then the Ca II absorption could represent the WIM around the WNM of Na I. However, because of the severe blending in these clouds, we must consider the b -values as very uncertain and this conclusion very tentative for these particular components.

The other three components (4, 10, and 12) are relatively free of line blending. Component 4, at -30 km s^{-1} , is the

strongest feature in the Ca II profile, and has the same b -value (4.6 km s^{-1}) for both Ca II and Na I. If we allow that in this case we have detected the coexistence of Ca II and Na I in the same environment, then the large and similar b -value implies that this cloud is dominated by turbulence and is a WNM environment. In § 3.1.2 we suggest that this component may be located near the star. Component 10 is a relatively weak and broad feature in both Na I and Ca II and is plausibly a WNM cloud. The Ca II b -value is smaller than Na I by a factor of 1.3, indicating that the region may be dominated by thermal broadening (the corresponding kinetic temperature would be $\sim 10,800 \text{ K}$). As we discuss in § 3.2.1, this component has an H I counterpart with a width consistent to the optical species. Component 12 consists of a hyperfine-resolved Na I and a broad Ca II. In this interesting case we propose that the Ca II absorption arises from the WIM component surrounding the CNM Na I, and where any corresponding CNM Ca II (which would be depleted on grains) is masked by broader intercloud Ca II. A similar situation was found by Barlow et al. (1995) for some of the clouds towards Zeta Ophiuchi.

Finally, we note that the weak, hfs Na I feature at 13.2 km s^{-1} , component 14, has a velocity difference of -0.7 km s^{-1} to a possible Ca II counterpart. Although this is a larger velocity difference than the other cases, the component may be another example, like component 12, of a CNM Na I core associated with warmer intercloud Ca II absorption.

3.1.1. The -11.1 km s^{-1} Component: Evidence for Variability

One of the most striking results of our new observation is the clear detection of a strong hfs-resolved Na I component at -11.1 km s^{-1} (component 9) which is absent in the earlier observations of SYH, see the middle panel of Figure 2. The component we detect at -11.1 km s^{-1} has an equivalent width of $10.7 \pm 0.8 \text{ m}\text{\AA}$ (2σ errors), while the very weak feature at the same velocity in the spectrum obtained by SYH is $1.7 \pm 1.5 \text{ m}\text{\AA}$ (which is barely significant at the 2σ level).

To our knowledge, there are only two other reported cases of comparable temporal variation in the strength of interstellar (as opposed to circumstellar) absorption lines. These are toward HD 72127 (Hobbs, Wallerstein & Hu 1982; Hobbs et al. 1991) and HD 72089 (Danks & Sembach 1995), both of which lie behind the Vela supernova remnant where small, fast moving clumps of material might be expected to intercept the line of sight. In the case of HD 28497 there is less reason to *expect* such spectacular line profile variations. We have considered two possible explanations, one circumstellar and one interstellar, as follows.

Given that HD 28497 has an IR excess, a circumstellar origin for this component seems at first sight the most plausible explanation for the spectral variability. However, this suggestion is weakened by the large velocity difference between this component (-11.1 km s^{-1}) and the stellar LSR radial velocity of -5.7 km s^{-1} . Moreover, both the extreme narrowness ($b = 0.31 \text{ km s}^{-1}$), and relatively high Na I/Ca II ratio [$N(\text{Na I})/N(\text{Ca II}) > 4.5$] of this component indicate an origin in cold unshocked material in which there is significant calcium depletion onto grain surfaces. Such conditions are more likely to be met in the cold interstellar medium than in the immediate vicinity of a Be star such as HD 28497.

As already noted, the line of sight to HD 28497 intercepts the expanding Orion-Eridanus shell, which Reynolds &

Ogden (1979) have intercepted as a possible supernova remnant. Further, as discussed in § 3.2.2, the line of sight passes close to an H I/IR filamentary structure and so might be expected to sample swept-up material with a high tangential velocity. We note that there is a difference between the variable component discussed here and those toward HD 72127; the latter had low Na I/Ca II ratios, indicative of shocked material in which Ca has been removed from the surfaces of grains (as would be expected for a supernova remnant or shocked gas in a filament), while the -11.1 km s^{-1} component toward HD 28497 has a high value for the ratio. On the other hand, the -11.1 km s^{-1} component may be closer to the case of the $+104 \text{ km s}^{-1}$ component toward HD 72089 which, as discussed by Danks & Sembach, showed a greater increase in the strength of Na I (at least a factor of 4) than in Ca II (a factor of 2.5) over a 10 yr period. In any case, if the -11.1 km s^{-1} component toward HD 28497 does arise in the Orion-Eridanus shell, then the feature must be a cold clump of gas in which most of the calcium atoms have remained (or been reabsorbed) on the surfaces of interstellar grains.

Of these two possible explanations, we propose that an interstellar origin is the more likely, with the variable -11.1 km s^{-1} component arising in a small, cold clump of interstellar gas associated either with the filamentary H I structure or the near side of the Orion-Eridanus shell. We recommend continued monitoring of the interstellar spectrum of this star, in the hope that the detection of additional line-profile changes will provide further clues to the origin of this component.

3.1.2. Comparison with Copernicus Data

From the *Copernicus* observations of Shull & York (1977), the absorption profile toward HD 28497 was shown to have two prominent features at -31.5 and -1.5 km s^{-1} , termed components A and B, respectively. An excitation temperature of 182 K for the B component and greater than 300 K for the A component were inferred from the relative populations of the $J = 0$ and $J = 1$ rotational levels of the ground vibrational state of H_2 . The velocity resolution of the *Copernicus* data is $\sim 14 \text{ km s}^{-1}$, and the absolute wavelength scale is accurate to $\pm 2 \text{ km s}^{-1}$, making the association of their B component (with $T_k \sim 182 \text{ K}$) to our Na I component 12 at $+3.1 \text{ km s}^{-1}$ (with $T_k \sim 190 \text{ K}$) firm. This provides a unique identification of warm H I gas containing H_2 (D. G. York private communication). As the H_2 and Na I coexist in the same CNM, we conclude that there is no turbulent broadening contribution to the observed Na I line width for this component.

More typically, kinetic temperature measurements obtained from H_2 studies result in values that are smaller than the corresponding values determined from the Na I line widths, even for the hfs-resolved components. From H_2 measurements reported by Savage et al. (1977), typical diffuse interstellar clouds have kinetic temperatures of $\sim 80 \text{ K}$ with a range between 50 and 130 K , and our ultra-high-resolution observations could detect temperatures in this range. Apart from component 12, the temperatures obtained from the other hfs Na I lines are a factor of 2 or so larger than H_2 values. This difference indicates that there are turbulent motions within the three other Na I components toward HD 28497.

Based on the rotational-level column density ratios of H_2 , Shull & York (1977) estimate for component A a high

value for the UV absorption rate and conclude that the cloud is probably located within 10 pc of HD 28497. Given the uncertainty in the *Copernicus* wavelength scale, we cannot establish unambiguously whether component A is associated with our component 4, which is a strong, broad, WNM cloud seen in both Ca II and Na I, or component 6 which is a CNM cloud seen prominently only in Na I (where it is hyperfine split). (Plausibly, components 4 through 7 could be part of the same interstellar environment, even though they are different and distinct phases.) However, we note that the low value of 0.25 for the Na/Ca ratio we obtain for component 4, and the large b -value, could be natural consequences of the cloud being close to the star, as the UV flux and stellar wind effects from the star would be substantial. The stellar ultraviolet flux can ionize gas-phase Na I, and also photodesorb trapped calcium atoms from the grain surfaces, while the stellar wind can sputter locked-up calcium atoms from the grains (Barlow & Silk 1977; Barlow 1978).

Since HD 28497 is known to have a circumstellar shell, we considered whether the -30 km s^{-1} component could be associated directly with this shell. From *Copernicus* studies of mass loss, Lamers & Snow (1978) found displaced Si IV absorption lines indicative of an outflow, and Snow, Peters, & Mathieu (1979) found evidence for a circumstellar shell through detection of the weak shell-line of Fe III at 1131 Å. The velocity determination for the shell is -145 km s^{-1} in the stellar rest frame, based on this single feature, and should be regarded as uncertain. (The velocity resolution of the data is $\sim 50 \text{ km s}^{-1}$.) The -30 km s^{-1} component is at roughly -35 km s^{-1} in the stellar rest frame and therefore does not appear to be associated directly with the material represented by the Fe III absorption in the shell of HD 28497. Our spectra do not cover the -145 km s^{-1} LSR region.

We attempted to match other interstellar species from *Copernicus* high-resolution data ($\sim 14 \text{ km s}^{-1}$) with our optical data. However, the absorption profiles measured by Shull & York (1977) are complex (hardly surprising in light of our UHRF data) and have a highly uncertain wavelength zero point. No useful comparisons, apart from the previously mentioned H₂ comparison, could be made. We shall attempt to obtain *HST* GHRS data toward HD 28497 later in 1996.

3.2. H I 21 cm Observations and Comparison with Optical Data

Large-scale mapping of H I in the Orion-Eridanus field, including the region around HD 28497, was carried out first by Heiles & Habing (1974), using an angular resolution of 30', a velocity resolution of 2 km s^{-1} , and a beam separation of ~ 0.3 for most cases. More detailed maps of the

distribution of neutral hydrogen and gas flow velocities for the region ($2^\circ \times 2^\circ$) around and including the dark cloud L1642, which includes MBM 20, were made by Taylor et al. (1982). Table 2 summarizes all the previous H I observations made toward this region and lists details of the observations in order to facilitate comparisons.

We have obtained H I 21 cm data from the Galactic survey made with the Dwingeloo 25 m telescope (Hartmann 1994; Hartmann & Burton 1995) for the region around HD 28497 in the velocity range -100 km s^{-1} to $+100 \text{ km s}^{-1}$. The telescope beam width used was 36' and the mean sensitivity of the data is about 0.07 K. The velocity resolution of these profiles is 1.03 km s^{-1} . Details of the observations and data reduction procedures can be obtained from the two references mentioned above.

Figure 3 shows H I line profiles at nine positions spaced 0.5 apart and clustered around HD 28497. We have fitted Gaussian profiles to the H I data and estimated velocities and column densities for the individual line components which are listed in Table 3 along with their positions. Column densities were estimated using equation (8-57) from Mihalas & Binney (1981), assuming that the material is optically thin and has a spin temperature of 100 K. We have compared our H I profiles to other published profiles, e.g., Taylor et al. (1982) at $(l, b) = (210^\circ 8, -36^\circ 7)$, Liljestrom & Mattila (1988) at the same position, Gir, Blitz, & Magnani (1994) at the position of MBM 20 which is $(l, b) = (210^\circ 8, -36^\circ 6)$, and the profile published by Lockman et al. (1986) at the position of HD 28497, and we obtain velocities that are consistent with these other data.

As can be seen from Figure 3, there are large variations in line strength from profile to profile. The overall velocity range of H I is similar to that found for the optical species, namely from -50 km s^{-1} to $+30 \text{ km s}^{-1}$, but individual features do not match up well. HD 28497 is located approximately between the two beams centered at positions 4 and 5 but does not fall within the FWHM of either. Figure 4 shows the position of HD 28497 with respect to the nine H I measurements.

The top panel of Figure 2 shows the H I profile at position 5 and the middle and lower panels show the Na D2 and Ca II K absorption profiles, respectively. The H I profile can be fitted by four Gaussian components: a broad component at -22.6 km s^{-1} , and three relatively narrow components at $-7.4, 6.6,$ and 12.2 km s^{-1} . The most important conclusion to emerge from this comparison is that with the exception of the -7.4 km s^{-1} component, the H I components do not seem to have Na I or Ca II counterparts at coincident velocities. We have further checked this as follows: we computed expected H I column densities for the four narrow hfs components using the observed relationship between $N(\text{H I})$ and $N(\text{Na I})$ (Hobbs 1984). The $N(\text{H I})$ range from

TABLE 2
SUMMARY OF PUBLISHED H I OBSERVATIONS

Authors	Beam Size (arcmin)	Velocity Resonance (km s^{-1})	Grid Spacing
Heiles & Habing 1974	30	2	15' in l 30' in b
Taylor et al. 1982	15	0.2	5'-15'
Liljestrom & Mattila 1988	9	0.42 and 1.69	4.5-9'
Gir et al. 1994	21	0.52	10'-20'
Hartmann & Burton 1995	36	1.03	0.5

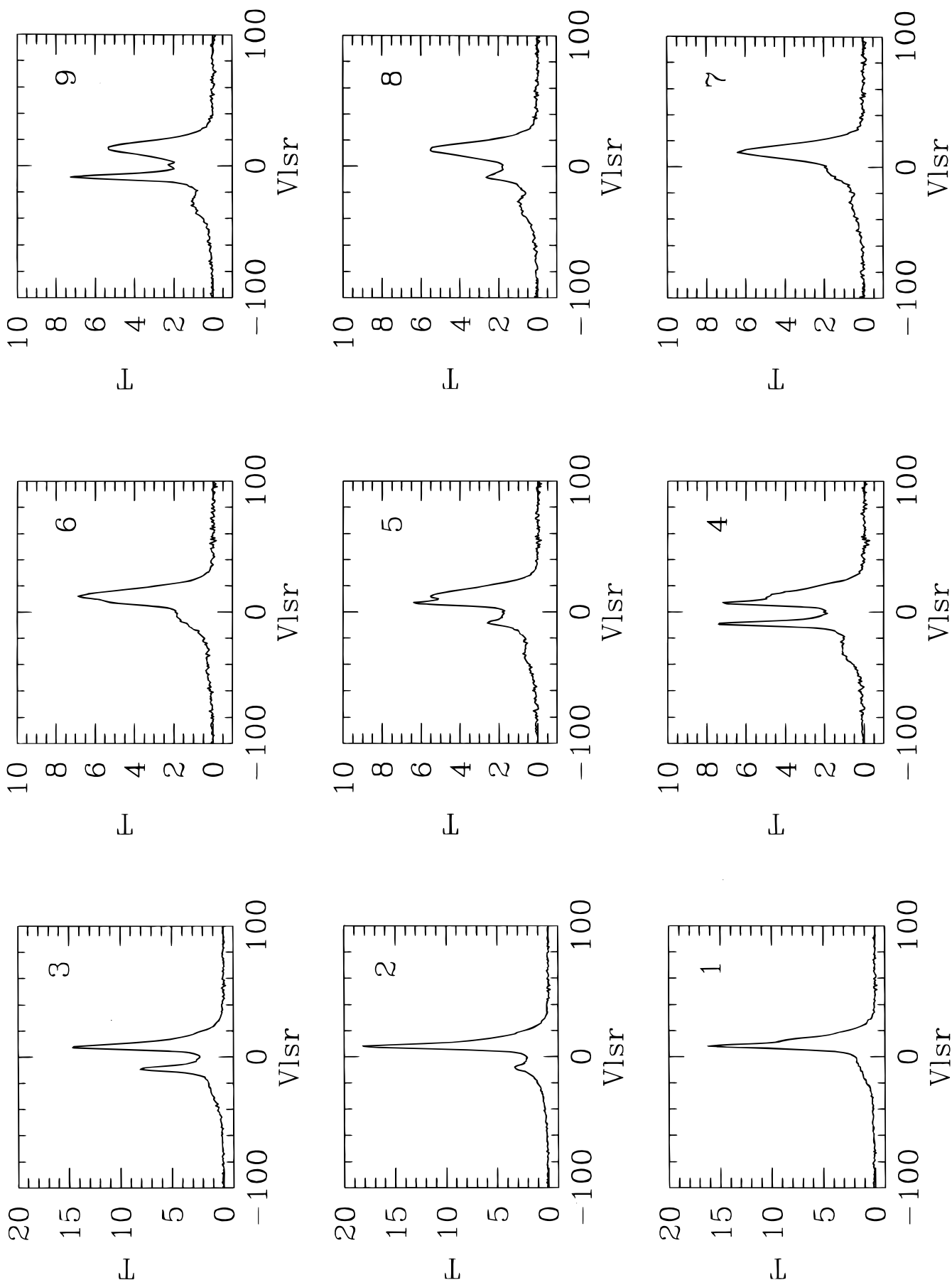


FIG. 3.—The H I profiles around HD 28497 from the Harmann & Burton (1997) survey are shown. Parameters of the Gaussian fits to the profiles are listed in Table 3. Note that except at position 1, no component corresponding to MBM 20 at km s^{-1} is seen, indicating that the line of sight to HD 28497 does not intersect this high-latitude molecular cloud.

TABLE 3
MODEL FIT PARAMETERS TO THE H I LINE PROFILES

Position	l, b	Velocity (km s ⁻¹)	FWHM (km s ⁻¹)	$N(\text{H I}) 10^{19} \text{ cm}^{-2}$
1	209°0, -37°0	-31.9	21.2	3.1
		-8.5	4.7	5.0
		2.8	34.7	13.5
		14.2	11.1	8.3
2	208°5, -37°0	-28.5	26.2	4.5
		-6.7	11.5	5.1
		12.6	14.5	15.8
		29.6	19.6	0.7
3	208°0, -37°0	-24.7	38.9	4.2
		-3.3	14.2	4.2
		10.7	10.3	7.2
		14.7	15.9	9.5
4	209°0, -37°5	-8.3	49.7	15.2
		-8.8	4.3	5.0
		6.7	2.9	2.1
		12.1	14.1	10.9
5	208°5, -37°5	-22.6	45.7	5.9
		-7.4	9.6	3.5
		6.6	2.6	1.4
		12.2	15.5	16.0
6	208°0, -37°5	-11.3	43.4	24.0
		10.4	9.5	5.8
		15.1	11.9	7.4
		-8.9	4.7	5.4
7	209°0, -38°0	-4.0	44.6	20.5
		7.7	4.4	9.2
		11.7	9.8	8.3
		-0.8	38.1	18.8
8	208°5, -38°0	7.8	4.1	11.1
		12.1	9.7	9.2
		2.9	38.8	14.0
		7.9	3.5	6.7
9	208°0, -38°0	11.6	10.6	14.7

0.9×10^{19} to 10^{21} cm^{-2} . Using the above N values and corresponding b -values, we constructed synthetic Gaussian profiles at the Na I velocities and found that in all four cases the corresponding H I components would have been detected.

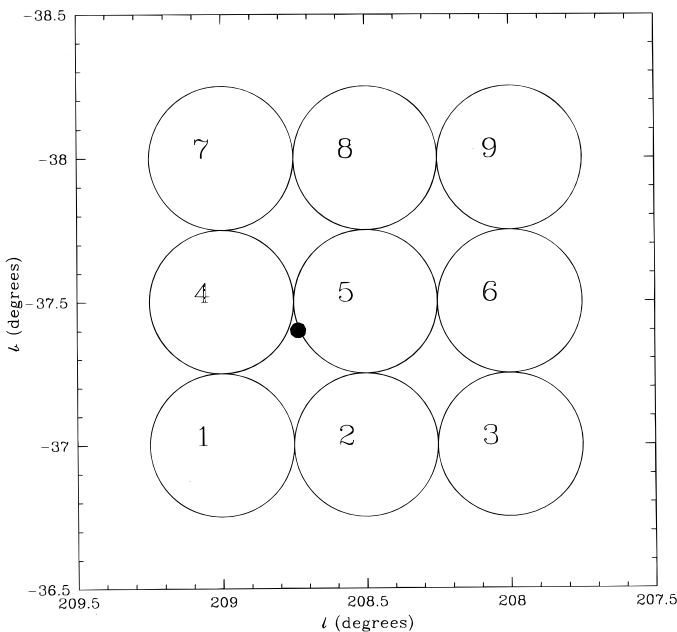


FIG. 4.—The position of HD 28497 with respect to the positions of the beams for the nine H I observations is shown. The star does not fall exactly into any of the nine beams and the closest is position 5.

There are three plausible reasons why the H I velocities do not match the Na I and Ca II velocities and we may have a combination of these reasons: first, the H I line has a larger intrinsic line width compared to Na I and Ca II; second, most of the H I emission is coming from beyond HD 28497; and third, the H I beam size being much larger than the beam size of the absorption measurements means that contributions from weak components having small angular extent can be lost among the general emission.

3.2.1. The -7.4 km s^{-1} Component: The Orion-Eridanus Loop

The -7.4 km s^{-1} H I component (nearest our component 10) seen in the profile at position 5 has a b -value of $\sim 12 \text{ km s}^{-1}$ which is approximately 4.8 times that of the width of the Na I absorption at the same velocity. This is what we would expect if the Na I and H I component were physically associated and if turbulent motions were not dominant. The temperature obtained from the Na I and H I data is consistent with a value of $\sim 10,000 \text{ K}$.

The H I feature has been associated with the Orion-Eridanus shell by Reynolds & Ogden (1979). Based on the intensity ratio between the H α and [N II] $\lambda 6584$ emission lines, these authors estimated an average $T_k = 8000 \pm 2000 \text{ K}$ for the entire Orion-Eridanus shell, with values ranging between 7400 and 18,000 K. If any of optical absorption components were indeed part of this expanding shell, we would expect the lines to be broadened predominantly by thermal motion, and hence the Ca line width would be smaller than the Na line width which is what we find (Table 1 and discussed in § 3.1). The radial velocity is also consistent with the observations of Reynolds & Ogden. Further,

the Na I/Ca II ratio for this component is 1.9, also consistent with what would be expected for a region at $\sim 10,000$ K (Bertin et al. 1993). This leads us to conclude that component 10 near -7.5 km s $^{-1}$ seen in the H I emission spectra and in the Na I and Ca II absorption spectra is associated with the front of the ionized expanding H α shell studied by Reynolds & Ogden.

3.2.2. -11.1 km s $^{-1}$ Component: The WNM Component with H $_2$

As discussed in § 3.1.1, we tentatively interpret the Na I hfs component at -11.1 km s $^{-1}$ to be a small cold cloud associated either with the near side of the Orion-Eridanus shell, as discussed above, or with the H I large-scale filamentary structure seen at velocities between -12 and -4 km s $^{-1}$. This H I filament has been associated on morphological grounds with a filament on an *IRAS* 100 μ m map which is offset in position by about $0^\circ.8$ (Verschuur et al. 1992). The H α emission shows that the ionized hydrogen also lies in filaments which are roughly parallel to the IR and H I filaments, but offset by 3 to 4° . The apparent separation of the gas and dust in the filamentary structure has been tentatively interpreted by these authors as due to variations in the clumping of the gas and dust on scales smaller than the H I and *IRAS* beams and to beam dilution effects.

3.2.3. MBM 20

From a comparison of the profiles at the 9 positions in Figure 3, the H I component of MBM 20 at ~ 0 km s $^{-1}$ weakens away from the core of the cloud. Close to the position of HD 28497 (positions 4 and 5) there is no prominent H I at ~ 0 km s $^{-1}$. This is consistent with the Na I and Ca II K absorption line profiles, which do not show any component at this velocity. Since the absorption profiles toward HD 28497 do not show a feature that can be associated with MBM 20, the line of sight must pass through clouds which are not physically associated with MBM 20. This is supported by the lack of detection of CH and CH $^+$ absorption (Penprase 1993) toward HD 28497.

4. CONCLUSIONS

We have made an ultra-high-resolution study (~ 0.32 km s $^{-1}$ resolution) of interstellar absorption lines toward the high galactic latitude star HD 28497. The main results can be summarized as follows.

1. Thirteen individual absorption components are detected in the Na I spectra and 10 in the Ca II K. Four Na I clouds show *s*-resolved hyperfine structure and would have kinetic temperatures in the range 134–227 K in the absence of turbulence. These cold, neutral phase gas clouds are not detected in Ca II. We attribute the broader Na I and Ca II features to warm neutral and/or warm ionized phases.

2. The narrow Na I component detected here at -11.1 km s $^{-1}$ was absent in the earlier spectra of SYH. The equivalent width of this component (10.7 ± 0.8 mÅ) is more than

5 times that of a barely significant feature at the same velocity in the earlier data. There seems little doubt that we have detected significant spectral change on a timescale of less than 20 yr. Tentatively, we attribute this component to a dense clump of interstellar gas associated with the foreground Orion-Eridanus shell or an H I filament, but note that a circumstellar origin cannot be entirely excluded.

3. Six components have the same velocities for both Na I and Ca II within the resolution of the data, although only three are relatively free of line blending, and we have considered whether the two species may coexist in these cases. The -30 km s $^{-1}$ component has a Ca II line width equal to the Na I line width, so this cloud plausibly originates in a region where turbulent motions dominate. Molecular hydrogen may also be present in this cloud with a high value for the UV absorption rate. The cloud has a low Na I/Ca II ratio ~ 0.25 . All of these observations are consistent with this cloud being located near HD 28497, as originally suggested by Shull & York (1977). The -7.5 km s $^{-1}$ component has a Ca II line width smaller than the Na I line width by a factor of 1.3, indicating that the region may be dominated by thermal broadening. A corresponding H I feature appears to be present at the same velocity and with a *b*-value consistent with the optical species. A kinetic temperature of $\sim 10,000$ K is derived for this component which may be associated with the front side of the large, expanding Orion-Eridanus shell. The third example consists of an hfs Na I feature associated with a broad Ca II. Here the Ca II may arise from a WIM component surrounding the CNM Na I, and where any corresponding CNM Ca II is masked by the broader Ca II component.

4. One of the purposes in studying HD 28497 was to use the star as a background probe of gas directly associated with the high galactic latitude molecular cloud MBM 20. However, we have not found evidence for this cloud in either the optical spectra or in the H I emission profiles nearest in location to MBM 20. Nevertheless, the ultra-high-resolution spectra that we have obtained provide important data on this complex interstellar direction and on the nature of the different phases of the ISM. We plan future observations of this star with the GHRM and STIS on the *HST* to explore the ultraviolet interstellar species. Future studies using the UHRF in this direction and others, where the individual interstellar components are neither saturated nor blended, will allow further insight into the nature of the interstellar medium.

We thank Dap Hartmann for kindly providing us with the H I profiles, L. M. Hobbs for helpful correspondence and the referee, Don G. York, for several important suggestions. I. A. C. thanks the STScI Visitors Program and L. H. thanks the STScI Graduate Student Program for financial support. M. S. S. is supported by the following *HST* grants, GO-3761 and GO-6723.

REFERENCES

- Abt, H. A., & Biggs, E. S. 1972, *Bibliography of Stellar Radial Velocities* (Tucson: Kitt Peak National Observatory)
- Ashok, N. M., Bhatt, H. C., Kulkarni, P. V., & Joshi, U. C. 1984, *MNRAS*, 211, 471
- Barlow, M. J., & Silk, J. 1977, *ApJ*, 211, L83
- Barlow, M. J. 1978, *MNRAS*, 183, 417
- Barlow, M. J., Crawford, I. A., Diego, F., Dryburgh, M., Fish, A. C., Howarth, I. D., Spyromilio, J., & Walker, D. D. 1995, *MNRAS*, 272, 333
- Bertin, P., Lallemand, R., Ferlet, R., & Vidal-Madjar, A. 1993, *A&A*, 278, 549
- Brown, A. G. A., Hartmann, D., & Burton, W. B. 1995, *A&A*, 300, 903
- Burrows, D. N., Singh, K. P., Nousek, J. A., Garmire, G. P., & Good, J. 1993, *ApJ*, 406, 97
- Danks, A. C., & Sembach, K. R. 1995, *AJ*, 109, 2627
- de Vries, C. P., Brand, J., Israel, F. P., de Graauw, Th., Wouterloot, J. G. A., van de Stadt, H., & Habing, H. J. 1984, *A&AS*, 56, 333
- Diego, F. 1993, *Appl. Opt.*, 32, 6284
- Diego, F., Fish, A. C., Barlow, M. J., Crawford, I. A., Spyromilio, J., Dryburgh, M., Brooks, D., Howarth, I. D., & Walker, D. D. 1995, *MNRAS*, 272, 323

- Gir, B.-Y., Blitz, L., & Magnani, L. 1994, *ApJ*, 434, 162
Goss, W. M., Manchester, R. N., Brooks, J. W., Sinclair, M. W., Manfield, G. A., & Danziger, I. J. 1980, *MNRAS*, 191, 533
Hartmann, D. 1994, Ph.D. thesis, Univ. Leiden
Hartmann, D., & Burton, W. B. 1997, *An Atlas of Galactic Neutral Hydrogen Emission* (Cambridge: Cambridge Univ. Press), in press
Heiles, C., & Habing, H. J. 1974, *A&AS*, 14, 1
Hobbs, L. M. 1984, *ApJS*, 56, 315
Hobbs, L. M., Ferlet, R., Welty, D. E., & Wallerstein, G. 1991, *ApJ*, 378, 586
Hobbs, L. M., Wallerstein, G., & Hu, E. M. 1982, *ApJ*, 252, 17
Lamers, H. G. L. M., & Snow, T. P. 1978, *ApJ*, 219, 504
Lesh, J. R. 1968, *ApJS*, 17, 371
Liljestrom, T. 1991, *A&A*, 244, 483
Liljestrom, T., & Mattila, K. 1988, *A&A*, 196, 243
Lockman, F. J., Hobbs, L. M., & Shull, J. M. 1986, *ApJ*, 301, 380
Magnani, L., Blitz, L., & Mundy, L. 1985, *ApJ*, 295, 402
McKee, C. F., & Ostriker, J. P. 1977, *ApJ*, 218, 148
McNutt, D. P., & Mack, J. E. 1963, *J. Geophys. Res.*, 68, 3419
Mihalas, D., & Binney, J. 1981, *Galactic Astronomy* (San Francisco: Freeman)
Morton, D. C. 1991, *ApJS*, 77, 119
Penprase, B. E. 1992, *ApJS*, 83, 273
———. 1993, *ApJS*, 88, 433
Reynolds, R. J., & Ogden, P. M. 1979, *ApJ*, 229, 942
Sandell, G., Johansson, L. E. B., Nguyen-Q-Rieu, & Mattila, K. 1981, *A&A*, 97, 317
Savage, B., Bohlin, R. C., Drake, J. F., & Budich, W. 1977, *ApJ*, 216, 291
Shull, J. M., & York, D. G. 1977, *ApJ*, 211, 803
Shull, J. M., York, D. G., & Hobbs, L. M. 1977, *ApJ*, 211, L139 (SYH)
Slettebak, A. 1982, *ApJS*, 50, 55
Snow, T. P., Peters, G. J., & Mathieu, R. D. 1979, *ApJS*, 39, 359
Taylor, M. I., Taylor, K. N. R., & Vaile, R. A. 1982, *Proc. Astron. Soc. Australia*, 4, 440
Verschuur, G. L., Rickard, L. J., Verter, F., Pound, M. W., & Leisawitz, D. 1992, *ApJ*, 390, 514
Welty, D. E., Hobbs, L. M., & Kulkarni, V. P. 1994, *ApJ*, 436, 152
Whitelock, P. A., Feast, M. W., & Catchpole, R. M. 1989, *MNRAS*, 238, 7P
York, D. G. 1996, private communication